



UNIVERSITY OF GRONINGEN

PHYSICS

BACHELOR RESEARCH PROJECT

Measurement of the Raw Asymmetry Ratio in the Decay $\Lambda_b^0 \rightarrow \Lambda^0 (\rightarrow p\pi^-) J/\psi (\rightarrow e^+e^-)$

Author:

Ludovica DE MARE
S4966996

First supervisor:

Ann-Kathrin PERREVOORT

Second supervisor:

Steven HOEKSTRA

January 26, 2025

Word Count	
Total Words:	1972
Headers:	15
Math Inline:	59
Math Display:	1
Close	

Abstract

It is essential to confirm that no CP violation (CPV) is observed in the $\Lambda_b^0 \rightarrow \Lambda^0 (\rightarrow p\pi^-) J/\psi (\rightarrow e^+e^-)$ decay in order to use it as a normalization channel for testing CPV in the $\Lambda_b^0 \rightarrow e^+e^-\Lambda^0$ decay. In this thesis, an analysis is conducted on LHC Run 2 data (years 2016–2018), corresponding to an integrated luminosity of 5.57 fb^{-1} , collected by the LHCb experiment from proton-proton collisions at $\sqrt{s} = 13 \text{ TeV}$. From the data, events compatible with the signal decay are selected and a suppression of the background process $B^0 \rightarrow J/\psi K_s^0$ based on kinematic properties is applied. In order to test for detection asymmetries, events taken at the two different polarities of the LHCb dipole magnet are analyzed, separately. Signal yields of Λ_b^0 and $\bar{\Lambda}_b^0$ along with the raw asymmetry ratio, are extracted through binned fits for each sample and the combined dataset. No detection asymmetry is observed and a raw asymmetry ratio of $A_{raw} = 0.029 \pm 0.032$ is measured for the combined dataset, leading to the conclusion that, in this study, no CP violation is observed in the decay.

Contents

1 Motivation	4
2 Theory	5
2.1 The Standard Model	5
2.2 The LHCb detector	5
2.3 $\Lambda_b^0 \rightarrow \Lambda^0 J/\psi$ decay	5
2.4 Invariant mass	5
3 Methods	6
3.1 Λ_b^0 candidate selection	6
3.2 Λ_b^0 cut veto	6
4 Results	9
5 Discussion	12
6 Conclusion	13
7 References	13
8 Appendix	13

1 Motivation

The Standard Model (SM) is the most successful quantum field theory we have in describing the laws that govern matter and its interactions at a fundamental level. However, this theory results incomplete since it fails in describing phenomena such as dark matter, the excess in the abundance of matter over antimatter in the universe or gravity.

In particular, the surplus in the abundance of matter over antimatter, also called matter–antimatter asymmetry, is a concept closely related to Charge-Parity Violation (CPV).

In particle physics, Charge-Parity (CP) conservation is the combined operation of Charge conjugation and Parity. Charge conjugation is conserved when an interaction between particles is invariant under the exchange of each particle with its antiparticle while Parity is conserved when a physical process and its mirror image have the same probability to happen in nature. Hence, a transformation in which CP symmetry is conserved swaps a particle with the mirror image of its antimatter particle, which is identical but has opposite quantum numbers.

Thus, the physical laws that govern nature cannot conserve CP symmetry entirely. If they did, the universe would contain an equal amount of particles and antiparticles which would have annihilated each other, leaving behind a universe filled mostly with radiation.

Within the Standard Model CP violation is observed in the weak interaction of particles such as K^0 , B^0 and D^0 mesons [1]–[3], with the latter observation being the first evidence of this asymmetry for the charm quark.

However, the CPV observed within the SM is not sufficient to explain the present-day matter–antimatter imbalance. For this reason, LHCb experiment at CERN is dedicated to high precision measurements of CP violation on rare b hadron decays, where, if an asymmetry were observed, it could potentially point to physics Beyond the Standard Model (BSM).

In this analysis, CP violation is investigated on the $\Lambda_b^0 \rightarrow J/\psi \Lambda^0$ decay, where $J/\psi \rightarrow e^+e^-$.

[...]

2 Theory

2.1 The Standard Model

[...]

2.2 The LHCb detector

[...]

2.3 $\Lambda_b^0 \rightarrow \Lambda^0 J/\psi$ decay

[...]

2.4 Invariant mass

[...]

3 Methods

3.1 Λ_b^0 candidate selection

A signal $\Lambda_b^0 \rightarrow J/\psi\Lambda$ decay candidate is reconstructed from a Λ^0 baryon and a J/ψ meson candidate. A signal candidate selection is applied on the data in order to distinguish this decay mode from other b-hadron decays with comparable final state products. In particular, only dielectron invariant mass squared q^2 compatible with a $J/\psi \rightarrow e^+e^-$ decay is considered i.e. $6 < q^2 < 11 \text{ MeV}^2$ [4].

3.2 Λ_b^0 cut veto

The Run 2 dataset from 2016–2018 is divided into two categories: long tracks (LL) and downstream tracks (DD), with each category further split into magnet up (MU) and magnet down (MD) data samples.

In this section Λ_b^0 cut veto analysis is conducted uniquely on DDMD data and the cut range found is applied to all data sets. Although the background shape is observed to be different, especially between LL and DD data, it is assumed that for the scope of this thesis, conducting the analysis for each different set, was not leading to a better final result or smaller uncertainty. Moreover, the DD data set has worse resolution than LL one, hence, starting with it to analyse the cut veto is considered the best choice.

Monte Carlo (MC) simulation is used to predict and check consistency of methods and results on data. MC simulation models background due to other decay modes and detector misidentification. In this analysis MC was used to study the $B^0 \rightarrow J/\psi K_s^0$ background decay with $K_s^0 \rightarrow \pi^+\pi^-$, where one of the pions is misidentified as a proton [5]. In order to distinguish among Λ^0 signal and K_s^0 background Equation ?? is used replacing the proton mass with the mass of the pion. By applying the modified version of the equation to the data the reconstructed K_s^0 mass distribution shown in Figure 1 is obtained, where the peak corresponds to the K_s^0 background, while the area around it to the signal.

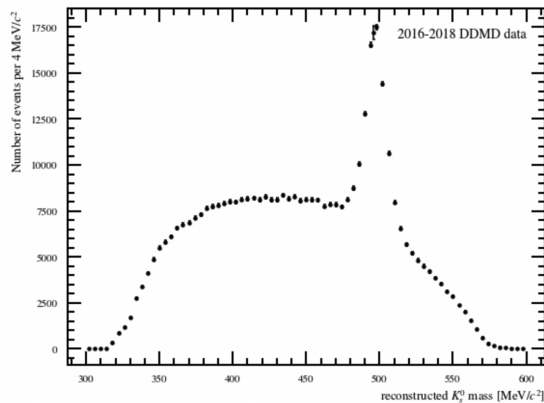


Figure 1: Reconstructed K_s^0 mass on DDMD data.

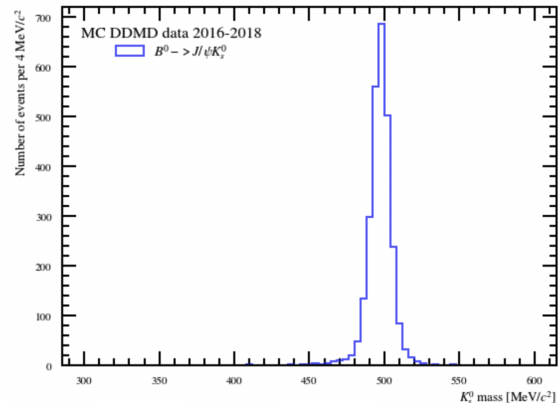


Figure 2: Simulated K_s^0 mass distribution on DDMD, MC data.

Different mass ranges are built using the reconstructed K_s^0 mass of simulated $B^0 \rightarrow J/\psi K_s^0$ events shown in Figure 2. The mean of this distribution, $\bar{m}_{K_s^0}^{rec} = 497 \text{ MeV}$ is used as the center

of symmetry and the standard deviation, $\sigma(m_{K_s^0}^{rec}) = 6.5$ MeV, to construct the widths of the ranges. As a result 40 ranges are defined in multiples of $\pm \frac{1}{3}$ of σ , or 2.2 MeV, around the mean of 497 MeV. Signal efficiency and background acceptance are calculated for each interval and displayed in Figure 3.

The range that maximally reduces the background and minimally affects the signal was chosen by calculating the gradient of the curve. A slope value less than 1 means that increasing the background acceptance leads to diminishing returns in terms of signal efficiency. Large veto ranges are found in the left part of the graph where the curve has a gradient larger than 1, whereas small veto ranges are found on the right side where the gradient is below 1. The gradient is calculated for the intermediate values to find the point where the increase in signal efficiency becomes smaller compared to the increase in background acceptance. This point is marked in red on the curve, which corresponds to a veto range of [483.8, 510.2] MeV, to a signal efficiency of 85% and to a background acceptance of 8%.

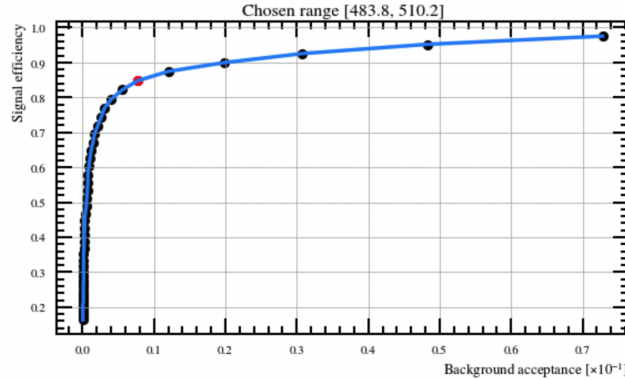


Figure 3: Signal efficiency and background acceptance values for each mass range. The mass range corresponding to the red data point is the one chosen for the cut veto.

Figure 4 and 5 show $\Lambda_b^0(\overline{\Lambda}_b^0)$ mass distributions before and after applying the veto. It is observed that while the cut preserves the shape of the signal, it effectively smooths the region just before the peak, where the K_s^0 contribution is expected to occur. It follows that the only remaining source of background is combinatorial.

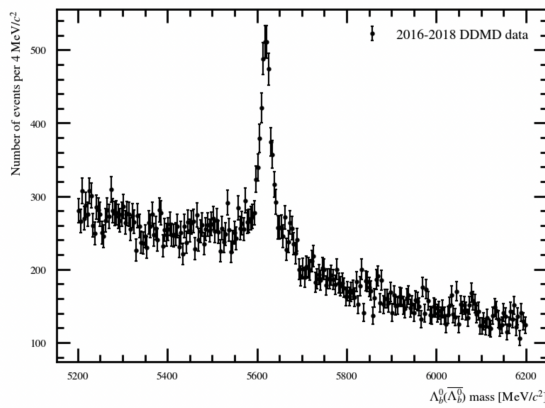


Figure 4: $\Lambda_b^0(\overline{\Lambda}_b^0)$ mass with q^2 selection applied, before cut on DDMD data.

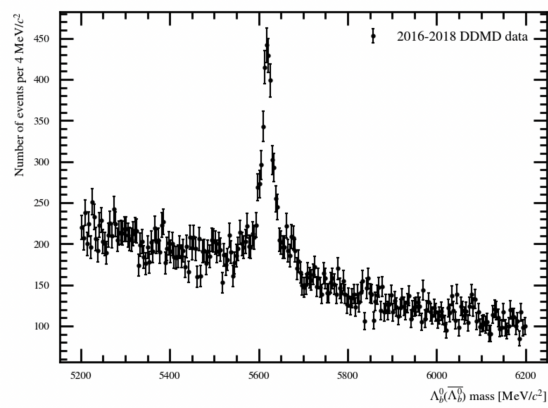


Figure 5: $\Lambda_b^0(\overline{\Lambda}_b^0)$ mass with q^2 selection applied, after cut on DDMD data.

4 Results

The signal yield is extracted through the sum of two Gaussian binned fits. A Gaussian probability density function is chosen to describe the core shape due to the main decay contribution, while the combination of two functions is used to take into account the broader contribution due to resolution effects.

The combinatorial background is fitted with an exponential function of the form ae^{-bx} , while the total fit is obtained by summing the signal and background fitting functions.

A selection is applied to the data to distinguish between Λ_b^0 and $\bar{\Lambda}_b^0$ particles, with different initial guesses calculated for each.

The signal fit initial parameters are derived from a preliminary fit on Monte Carlo simulated data, while those for the combinatorial background fit are obtained by applying the exponential function to the background regions only of the data distributions.

The same procedure is applied to determine the signal yield across all four samples and the binned data fits for each of them are presented in the plots shown in Figures 6 to 13.

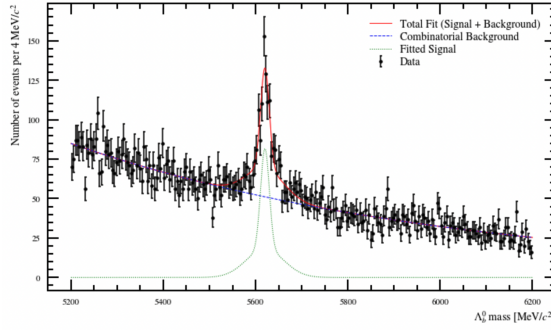


Figure 6: LLMD particle data.

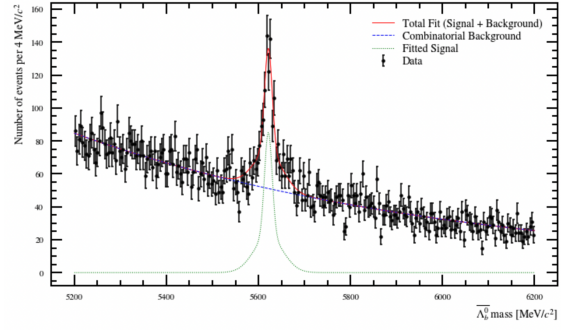


Figure 7: LLMD antiparticle data.

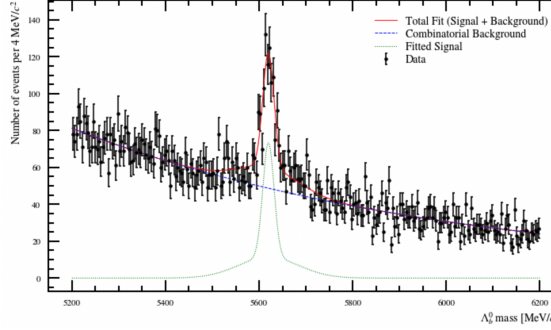


Figure 8: LLMU particle data.

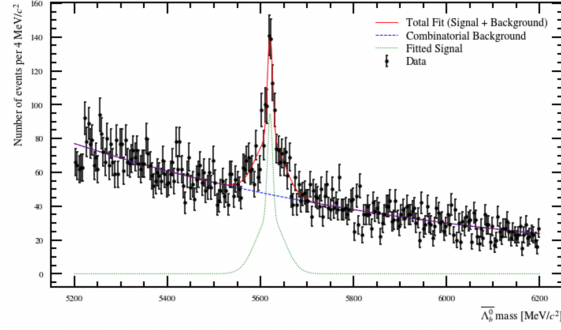


Figure 9: LLMU antiparticle data.

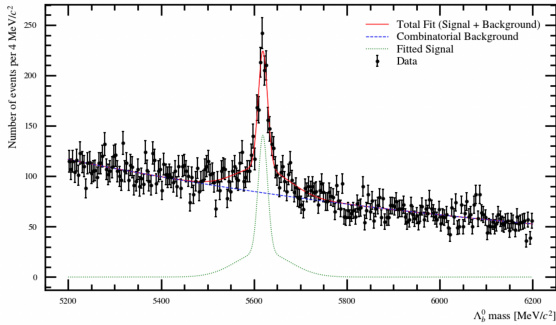


Figure 10: DDMD particle data.

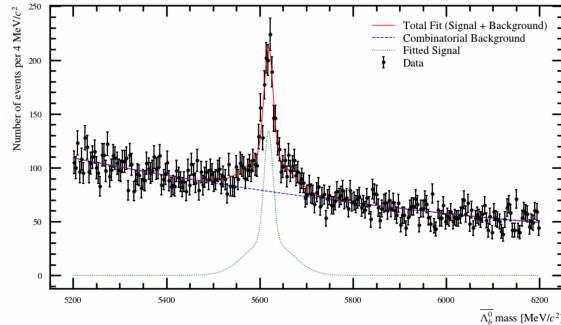


Figure 11: DDMD antiparticle data.

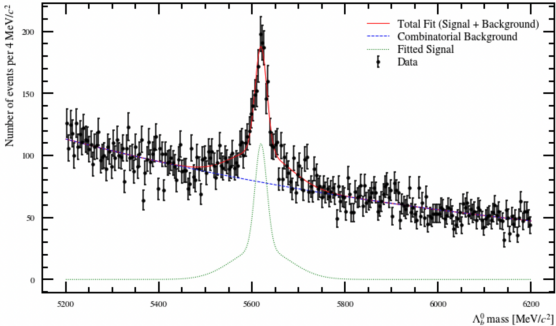


Figure 12: DDMU particle data.

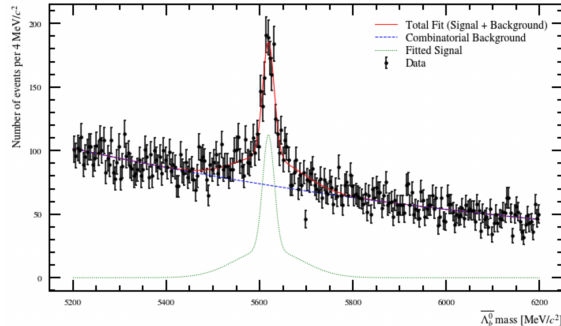


Figure 13: DDMU antiparticle data.

Furthermore, by combining the four data samples, the plots in Figures 14 and 15 are obtained.

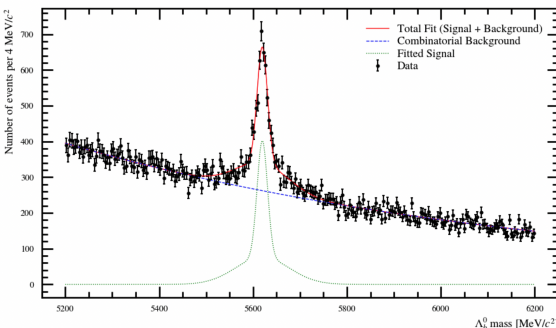


Figure 14: Particle selection on all DDMU, DDMD, LLMU, LLMD data.

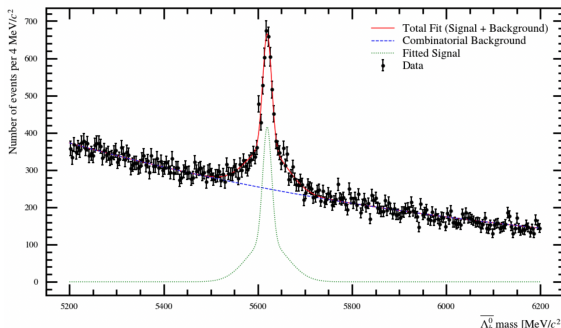


Figure 15: Antiparticle selection on all DDMU, DDMD, LLMU, LLMD data.

Two normalization parameters are used for the two Gaussian PDFs. The sum of these optimal values, divided by the bin width, provides the total signal yield for each plot, as shown in Table 1. Each value is displayed with its standard deviation.

The raw asymmetry ratio defined by the following equation:

$$A_{\text{raw}} = \frac{N_{\Lambda_b^0} - N_{\bar{\Lambda}_b^0}}{N_{\Lambda_b^0} + N_{\bar{\Lambda}_b^0}} \quad (1)$$

is calculated for each sample along with its associated uncertainty. This raw asymmetry includes contributions from different sources of asymmetry. The three main contributors to the raw asymmetry are: production asymmetry, decay asymmetry and detection asymmetry.

Production asymmetry arises from the proton-proton initial state from which more Λ_b^0 than $\bar{\Lambda}_b^0$ particles are expected to be produced [6].

Detection asymmetry stems from systematic effects in the detector, such as differences in efficiency when detecting particles versus antiparticles, variations in resolution or reconstruction biases. These latter effects are experimental artifacts rather than true physical asymmetries.

Lastly, the physical asymmetry in the decay process itself, which could potentially point to CP violation, is also a factor.

However, this ratio is considered an effective choice to investigate matter-antimatter asymmetry as systematic effects that similarly impact both particle and antiparticle measurements largely cancel out.

	Λ_b^0	$\bar{\Lambda}_b^0$	A^{raw}
LLMD	835 ± 94	760 ± 99	0.047 ± 0.086
LLMU	924 ± 105	842 ± 68	0.046 ± 0.069
DDMD	1620 ± 132	1612 ± 112	0.002 ± 0.053
DDMU	1635 ± 139	1690 ± 135	-0.016 ± 0.058
All samples	4983 ± 241	4696 ± 199	0.029 ± 0.032

Table 1: Signal yields and asymmetries for different data samples.

5 Discussion

The total fit of all data sets converges to both the signal and background effectively, allowing to extract the signal yields for both particle and antiparticle decays as shown in the Table 1. Initially, the signal was fitted using a Double-Sided Crystal Ball function [5], [7], where one side mirrors the other. The results of this attempt are presented in the Appendix. However, due to the complexity of the numerous parameters involved, this fit produced less accurate results, with uneven standard deviations between the Λ_b^0 and $\bar{\Lambda}_b^0$ number of events. Consequently, the sum of two Gaussian functions was deemed a better choice for the signal fit, as it consistently reproduces the signal peaks and event counts for the Λ_b^0 and $\bar{\Lambda}_b^0$ masses across all datasets, with mass distributions centered around the expected value of 5619 MeV.

By comparing the LL and DD plots, it is observed that the signal fit shapes are quite similar across the different data sets. A broader signal peak, and thus a larger standard deviation, was expected in the DD sample due to its poorer resolution compared to the LL sample. However, this effect is not observed, very likely because the post-bremsstrahlung-correction momentum resolution of the electrons is dominating the mass resolution of Λ^0 . In addition, the higher number of events in the DD sample compared to the LL sample indicates that more Λ^0 particles are detected decaying outside the VELO than within the region.

Moreover, by comparing MU and MD samples it is possible to investigate the possibility of a detection asymmetry. When the MU polarity is used to detect particles, positive decay products are bent upwards while negative particles are bent downwards. If a detection asymmetry is present, i.e. different detection efficiencies for particles moving in different directions, the bias will manifest in opposite ways when the magnet polarity is switched.

By comparing the number of events between the MD and MU samples in Table 1, no conclusive detection asymmetry can be observed in either the LL or DD samples, as the event counts are within one standard deviation of each other.

Finally, the total number of Λ_b^0 and $\bar{\Lambda}_b^0$ particles in the decay is presented in the combined 'all samples' category. As expected, the increased statistics in this category results in reduced uncertainties compared to the DD and LL samples. The raw asymmetry ratio, along with its propagated uncertainty, is shown in the last row and column of Table 1.

The latter value lies within its uncertainty range, indicating no evidence of a matter-antimatter asymmetry. This result is consistent with expectations, as the studied decay is described by a tree-level Feynman diagram, where, contrarily to higher-order diagrams, CP violation is not typically observed. It follows that the decay studied is a good candidate as a normalization channel for the $\Lambda_b^0 \rightarrow e^+e^-\Lambda^0$ decay, which is indeed described by an higher order Feynman diagram.

Finally, this analysis could be further improved by the use of unbinned fits. Indeed, signal yields and raw asymmetries can be determined for example with the use of unbinned maximum-likelihood fits to invariant mass distributions [6]. The maximum-likelihood fit is a statistical method used to model data and extract the most likely number of signal events while accounting for the background events. In this context, the fitting function might include parameters that describe both the signal and the background so that background due to particle misidentification is actually fitted along with the signal and not removed by veto from the data.

To conclude, analysis and understanding of systematic uncertainties would be beneficial to the solidity of the final results.

6 Conclusion

[...]

7 References

[...]

8 Appendix

[...]